Synlett

Accounts and Rapid Communications in Chemical Synthesis

Supporting Information

for DOI: 10.1055/s-0043-1775482

Georg Thieme Verlag KG, Oswald-Hesse-Straße 50, 70469 Stuttgart, Germany

Thieme

Supporting Information

An Azobenzene-Bipyridinium Derivative as Component in the Construction of Photoresponsive Pseudorotaxanes

Leonardo Andreoni[a,b], Dalila Cafagno[b,c,d], Alberto Credi*[a,b], Jessica Groppi*[b,e]

[a] Dipartimento di Chimica Industriale "Toso Montanari", Università di Bologna, via P. Gobetti 85, 40129 Bologna, Italy.

[b] CLAN-Center for Light Activated Nanostructures, Institute ISOF-CNR, via P. Gobetti 101, 40129 Bologna, Italy.

[c] Dipartimento di Chimica, Biologia e Biotecnologie, Università degli Studi di Perugia, via Elce di Sotto 8, 06123, Perugia, Italy.

[d] Dipartimento di Chimica "G. Ciamician", Università di Bologna, via Selmi 2, 40126 Bologna, Italy.

[e] Institute for Organic Synthesis and Photoreactivity (ISOF), National Research Council of Italy (CNR), via P. Gobetti 101, 40129 Bologna, Italy.

E-mail: jessica.groppi@cnr.it, alberto.credi@unibo.it

Table of contents

1. Material and Methods

General Synthesis Information. 4-nitrosotoluene[i] and 1,1'-bis(2,4-dinitrophenyl)-4,4'-bipyridinium dichloride[ii] were synthesized according to literature procedures. All reagents and chemicals were purchased from Merck, VWR international or Fluorochem and used as received unless otherwise stated. Solvents were dried according to literature procedures. Thin layer chromatography was performed on TLC Silica gel 60 F254 coated aluminium plates from Merck. Flash column chromatography was performed using Merck Silica 40 (230-400 mesh size or 40-63 mm) as the stationary phase.

NMR Spectroscopy. NMR spectra were recorded on an Agilent DD2 spectrometer operating at 500 MHz. Chemical shifts are quoted in part per million (ppm) relative to tetramethylsilane using the residual solvent peak as a reference standard and all coupling constants (*J*) are expressed in Hertz (Hz).

NMR Photochemistry. Photochemical reactions were performed in air-equilibrated solutions at 298 K inside NMR tubes within the spectrometer probe-head, using a Prizmatix UHP-T-365-SR LED Illuminator (1.5 W, λ_{max}= 369 ± 5 nm, FWHM 15.56 nm) equipped with an FCASMA adaptor for optical fiber. Quartz optical fiber (core 1000 μm, 5 m) equipped with a SMA connector on one end was purchased from Thorlabs. The other end of the optical fiber was freed of the protective coatings, exposing 6 cm of the quartz core, and sanded to uniformly diffuse light in the solution. The exposed quartz fiber was submerged into the solution (V = 0.5 ml) within the NMR tube to be irradiated.

UV-Vis Spectroscopy. UV-vis absorption spectra were recorded with Cary 300 (Agilent) and a lambda750 (Perkin Elmer) spectrophotometers. Measurements were performed on air-equilibrated acetonitrile (Sigma-Aldrich) solutions at room temperature (298 K) in the presence of BHT (1 mM). All solutions were prepared and examined in a dark room illuminated only by a red light to avoid undesired photoisomerisation of the investigated compounds. Irradiation experiments were performed with a LOT-QuantumDesign (200 W) medium-pressure mercury lamp at room temperature (298 K). The photoisomerisation quantum yields were determined with a diode array Avantes photometer equipped with an

optical fibre and coupled to the LOT-QuantumDesign medium-pressure mercury lamp. This setup allows to record the absorption spectra under continuous irradiation. The desired Hg emission line was selected with an interference filter (Edmund Optics, OD 4.0 10nm Bandpass Filter). The incident light intensity was measured for each experiment using the dimethylazobenzene actinometer.[iii] The solutions were carefully stirred throughout the whole irradiation to ensure the homogeneity of the solution. The photoisomerisation quantum yields were determined by fitting the time-dependent absorption changes with the model for a T-type photochrome[iv] using Berkeley-Madonna.[v] The quantum yields were determined at least on two different samples of the same compound and the values were averaged. The experimental error on the quantum yield values was estimated to be ±10%. The absorption spectrum of the *Z* isomer was determinated by the Fischer method[2] from the photostationary states obtained upon irradiation at 313 nm and 365 nm. Thermal back isomerisation kinetics measurements were performed on previously irradiated solutions kept in the dark by monitoring the absorbance variations over time at room temperature (298 K).

2. Synthetic Procedures

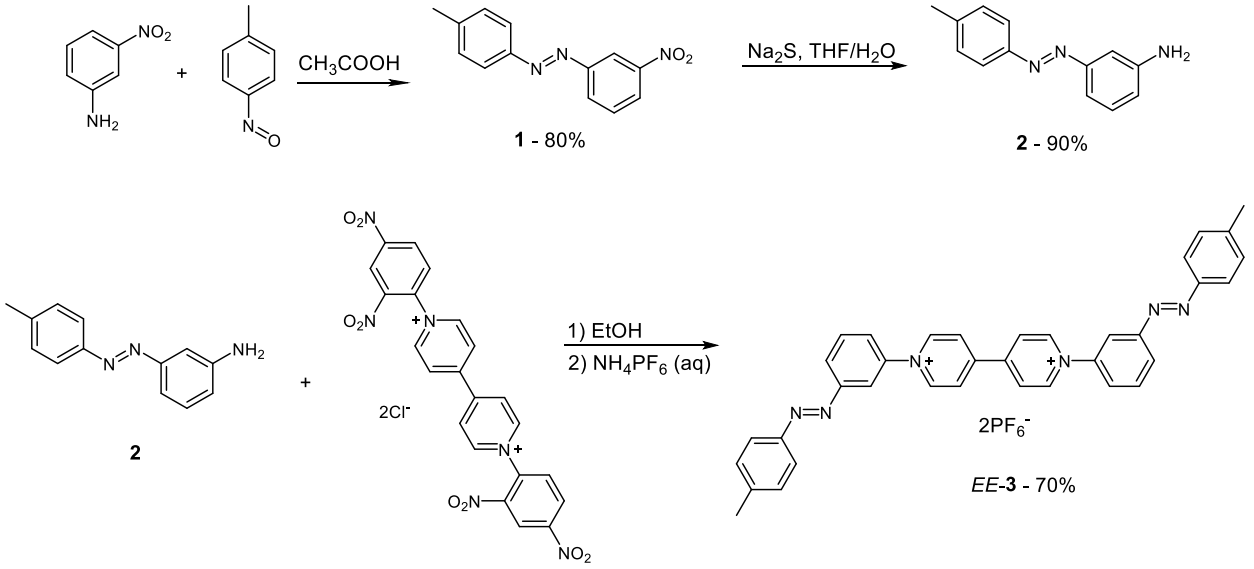

Scheme S1. Synthetic steps to compound *EE*-**3**.

(E)-1-(3-nitrophenyl)-2-(p-tolyl)diazene (1)

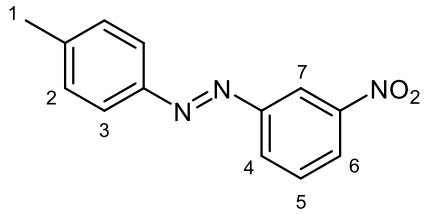

Nitrosotoluene (1.00 g, 8.3 mmol) and 3-nitro-aniline (0.86 g, 6.2 mmol) were dissolved in acetic acid (20 ml) and left stirring at room temperature for 72 hours. water (50 ml were added to the reaction mixture to precipitate the crude product as light brown solid. The product was purified over silica column, eluent Hexane (Hex) : Ethyl Acetate (EtOAc) (90:10). The product was an orange solid, obtained in 80 % yield (1.20 g). **^{1}H NMR** (500 MHz, $CDCl_3$, 298 K) δ = 8.72 (s, 1H, H_7), 8.31 (d, *J*= 8.1 Hz, 1H, H_6), 8.24 (d, *J*=7.9 Hz, 1H, H_4), 7.88 (d, *J*=8.1 Hz, 2H, H_3), 7.69 (t, *J*=8.0 Hz, 1H, H_7), 7.35 (d, *J*=8.1 Hz, 2H, H_2), 2.46 (s, 3H, H_1). **^{13}C NMR** (125 MHz, $CDCl_3$, 298 K) δ = 153.3, 150.5, 149.2, 143.1, 130.1, 130.0, 129.3, 124.7, 123.5, 117.1, 21.8.

(E)-3-(p-tolyldiazenyl)aniline (2)

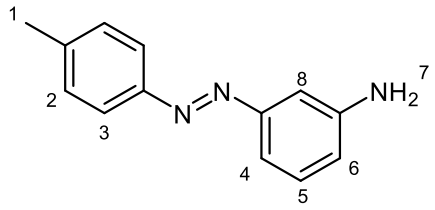

Compound **1** (0.52 g, 2.1 mmol) was dissolved in tetrahydrofuran (THF, 25 ml) and an aqueous solution (10 ml) of sodium sulfide nonahydrate ($Na_2S.9H_2O$, 3 g, 12 mmol) was added. The mixture was stirred vigorously at reflux temperature for 48 hours. The residual THF was removed, and a solution of sodium hydroxide (NaOH 2 M aq., 25 ml) was added. The aqueous phase was extracted with EtOAc (2x50 ml). The organic extracts were combined, dried over sodium sulfate and the solvent was removed The product was purified over silica column, eluent Hex : EtOAc (70:30). The product was an orange solid obtained in 93% yield (0.42 g). **^{1}H NMR** (500 MHz, $CDCl_3$, 298 K) δ = 7.81 (d, *J*=8.3 Hz, 2H, H_3), 7.35-7.28 (m, 4H, H_2+H_4+H_5), 7.20 (s, 1H, H_8), 6.80 (d, *J*=6.5 Hz, 1H, H_6), 3.81 (bs, 2H, H_7), 2.43 (s, 3H, H_1). **^{13}C NMR** (125 MHz, $CDCl_3$, 298 K) δ = 147.3, 129.9, 122.9, 117.7, 115.1, 107.5, 21.6.

1,1'-bis(3-((E)-p-tolyldiazenyl)phenyl)-[4,4'-bipyridine]-1,1'-diium (*EE*-3)

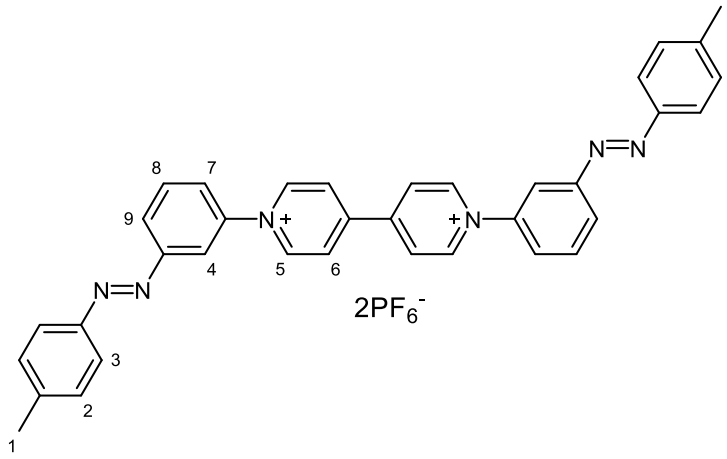

1,1'-bis(2,4-dinitrophenyl)-4,4'-bipyridinium dichloride (0.5 g, 0.8 mmol) and compound **2** (0.4 g, 1.8 mmol) were dissolved in ethanol (EtOH, 40 ml) and the solution was stirred at reflux temperature for 48 hours. The solvent was removed, and the solid residue was dissolved with water 50 ml and EtOAc (50 ml). The aqueous phase was extracted with EtOAc three times (3x50 ml). A saturated solution of ammonium hexafluorophosphate (NH_4PF_6 aq) was added to the aqueous phase, which contained the chloride salt of the product, to precipitate the product as the hexafluorophosphate salt. The solid was filtered and washed with water and EtOH, then dried under vacuum. The product was an orange solid obtained in 71% yield (0.5 g). **^{1}H NM**R (500 MHz, CD_3CN, 298 K) δ = 9.30 (d, *J*=6.5 Hz, 2H, H_5), 8.71 (d, *J*=6.5 Hz, 2H, H_6), 8.31 (d, *J*=8.0 Hz, 2H, H_7), 8.29 (s, 1H, H_4), 7.98 (t, *J*=8.0 Hz, 1H, H_8), 7.93-7.90 (m, 3H, H_3+H_9), 7.45 (d, *J*=8.2 Hz, 2H, H_2), 2.47 (s, 3H, H_1). **^{13}C NMR** (125 MHz, CD_3CN,

298 K) δ = 154.6, 151.6, 151.3, 146.9, 144.7, 144.1, 132.8, 131.2, 128.5, 127.7, 127.3, 124.1, 118.8, 21.6. **^{19}F NMR** (470 MHz, CD_3CN, 298 K) δ -73.00 (d, *J* = 706.4 Hz).

3. NMR Characterization

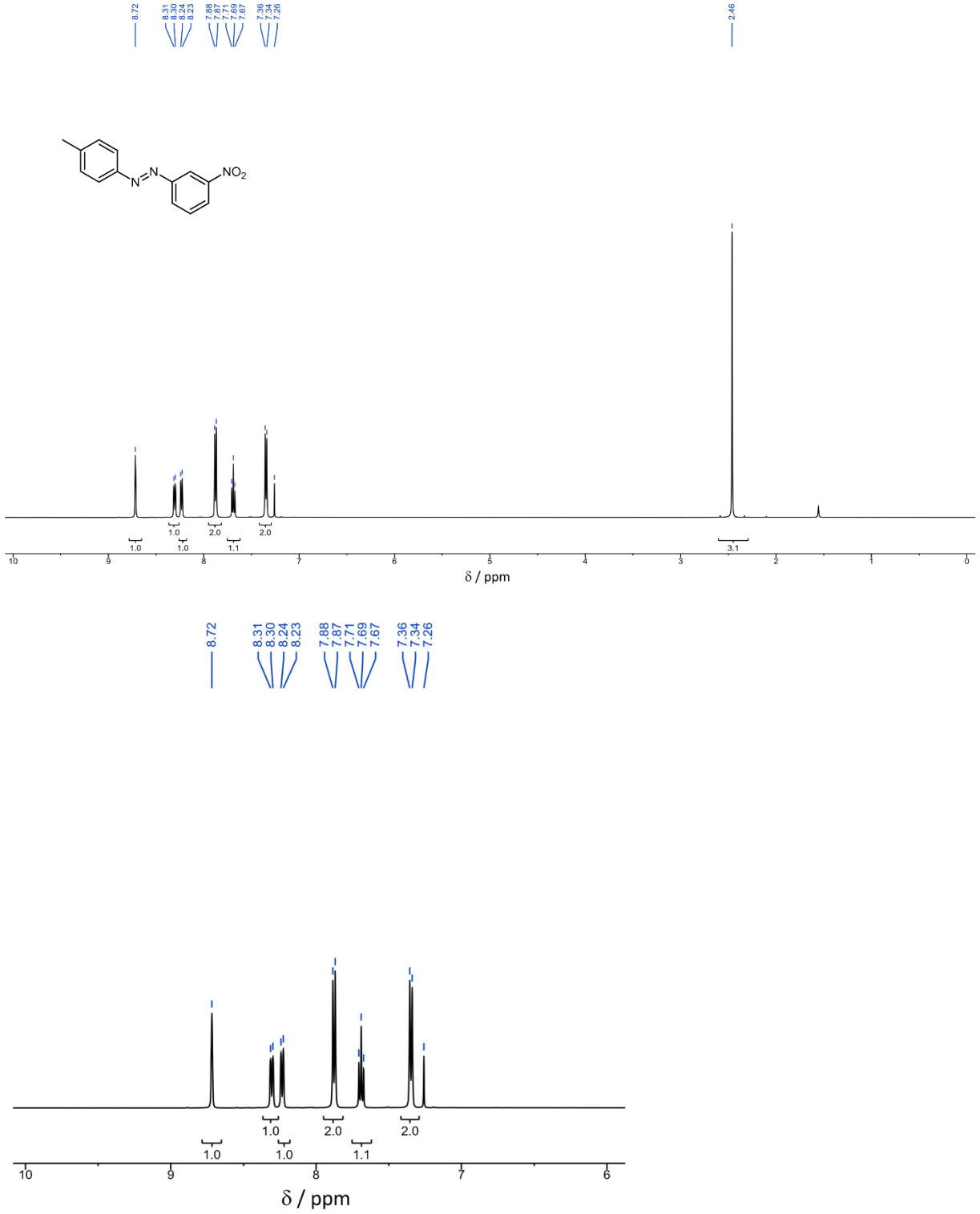

Figure S1. ^{1}H NMR spectrum (500 MHz, $CDCl_3$, 298 K) of compound **1**. Top: full spectrum; Bottom: expansion of the aromatic region.

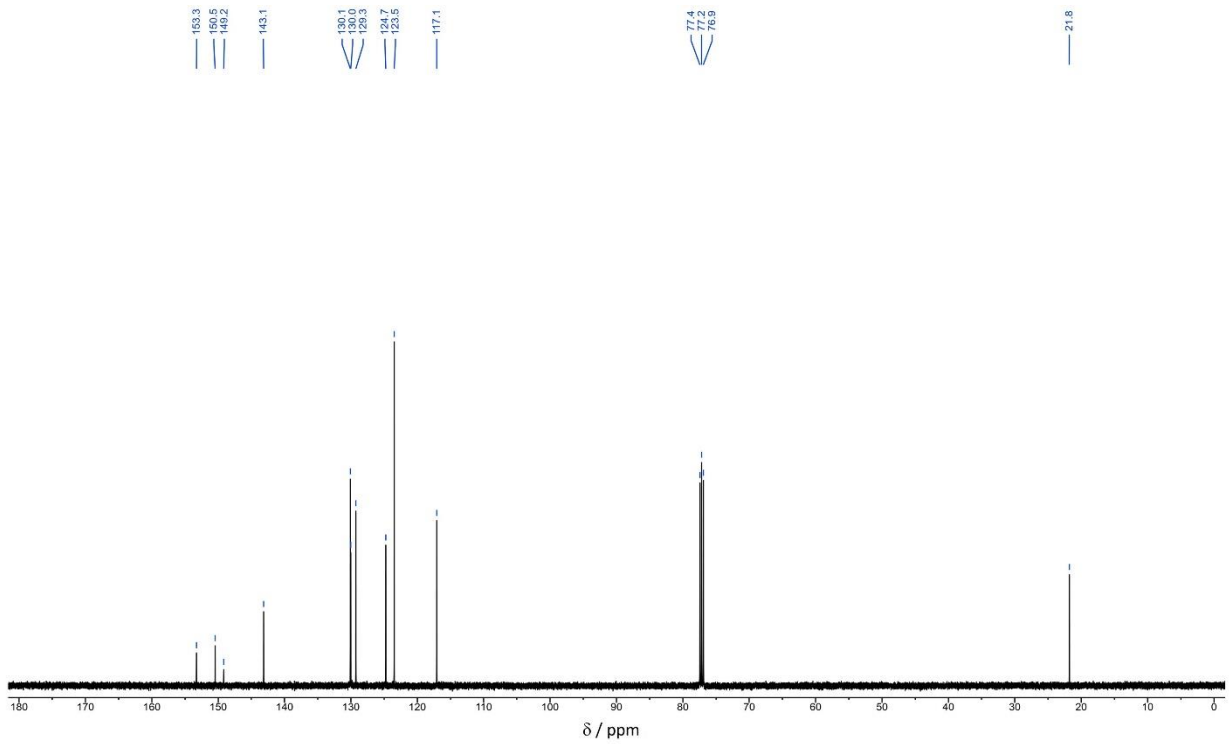

Figure S2. ^{13}C NMR spectrum (125 MHz, $CDCl_3$, 298K) of compound **1**.

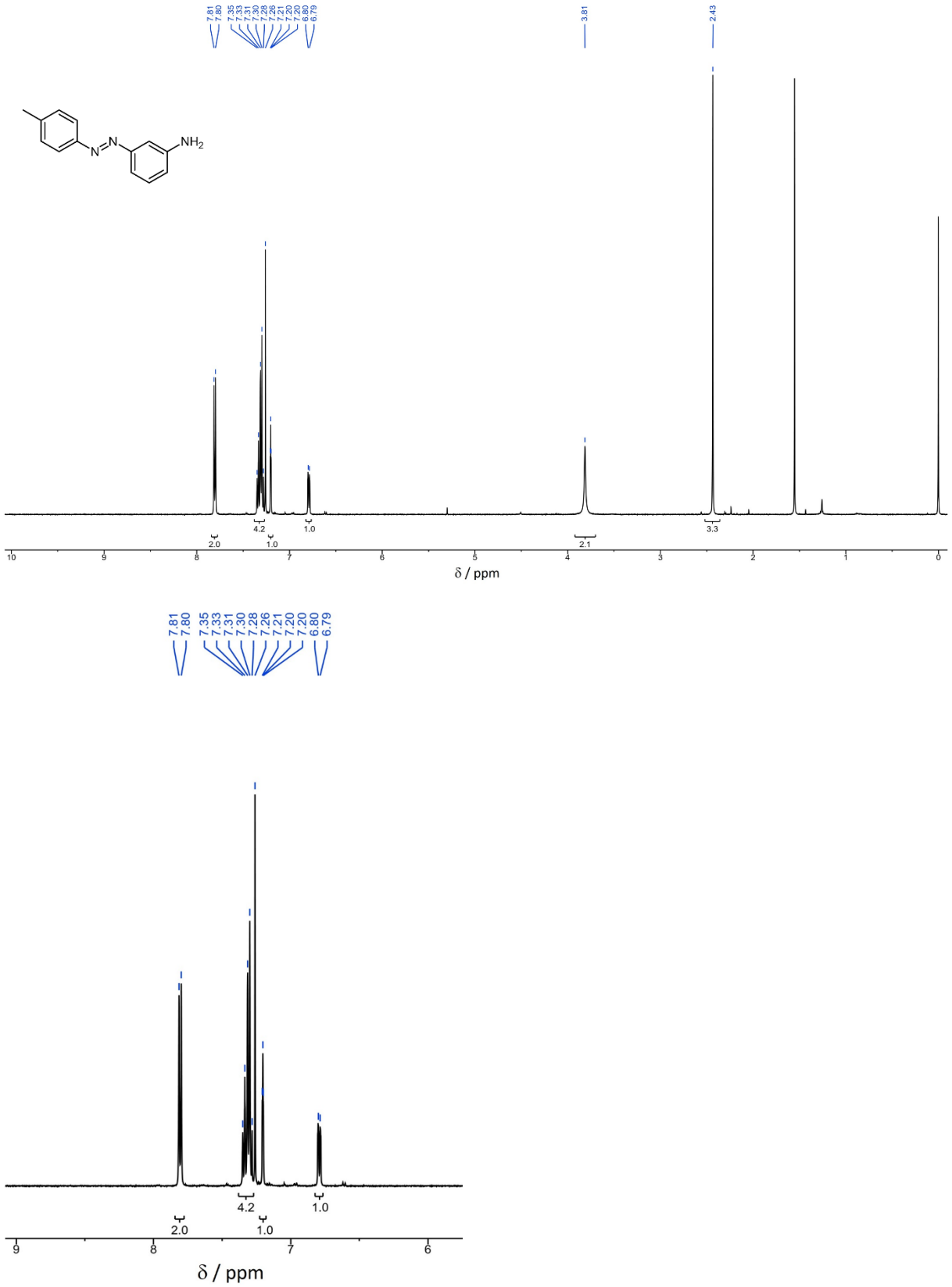

Figure S3. ^{1}H NMR spectrum (500 MHz, $CDCl_3$, 298 K) of compound **2**. Top: full spectrum; Bottom: expansion of the aromatic region.

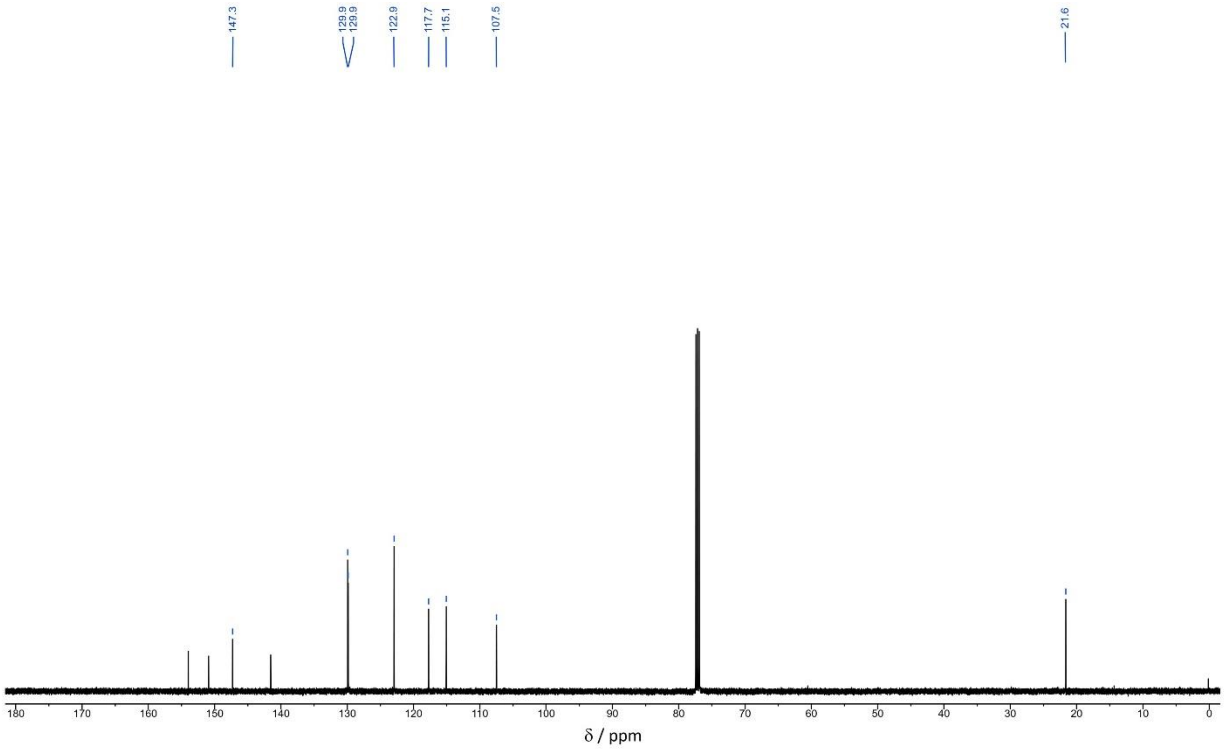

Figure S4. ^{13}C NMR spectrum (125 MHz, $CDCl_3$, 298K) of compound **2**.

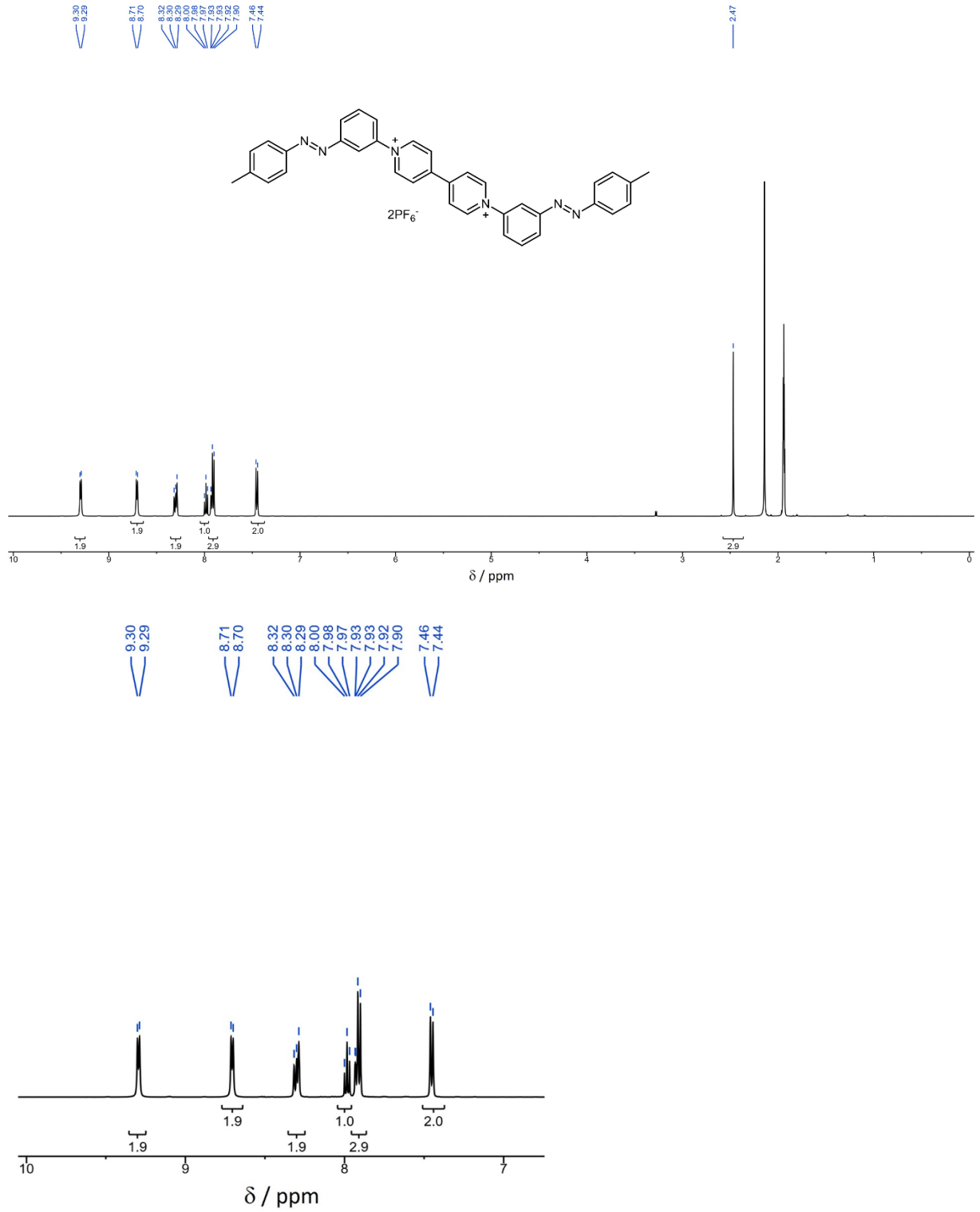

Figure S5. ^{1}H NMR spectrum (500 MHz, CD_3CN, 298 K) of compound *EE*-**3**. Top: full spectrum; Bottom: expansion of the aromatic region.

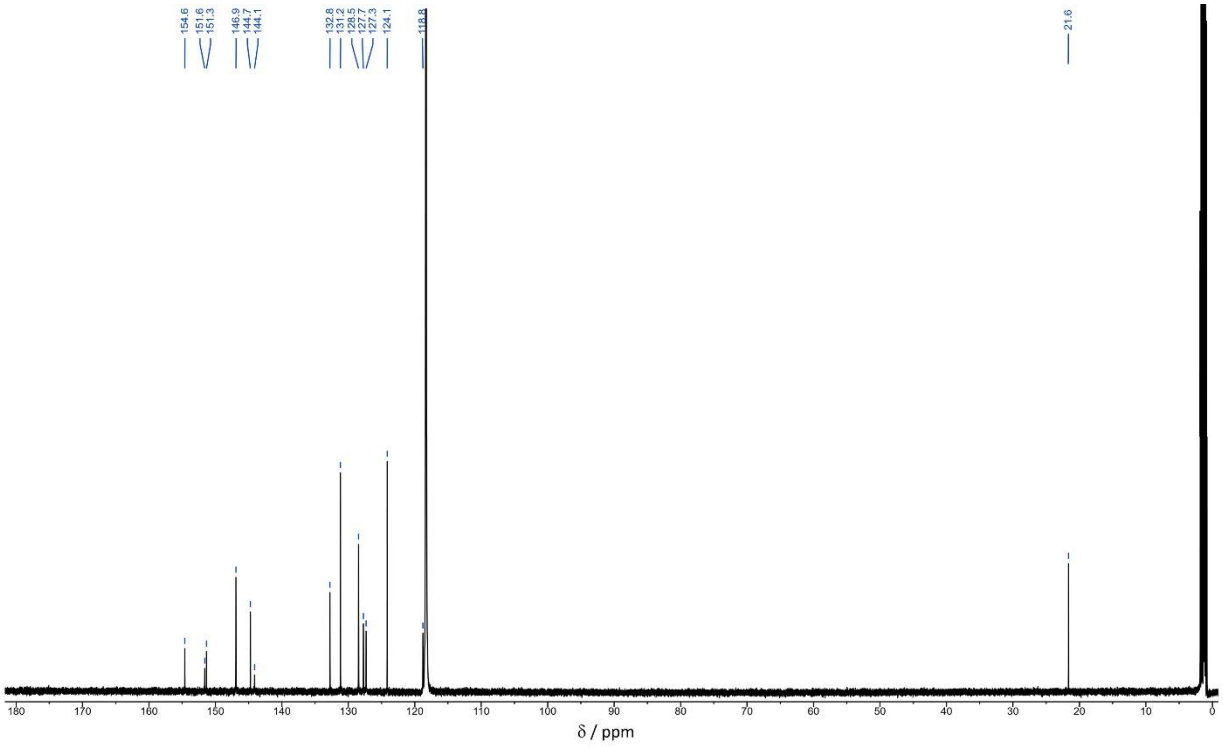

Figure S6. ^{13}C NMR spectrum (125 MHz, CD_3CN, 298K) of compound *EE*-**3**.

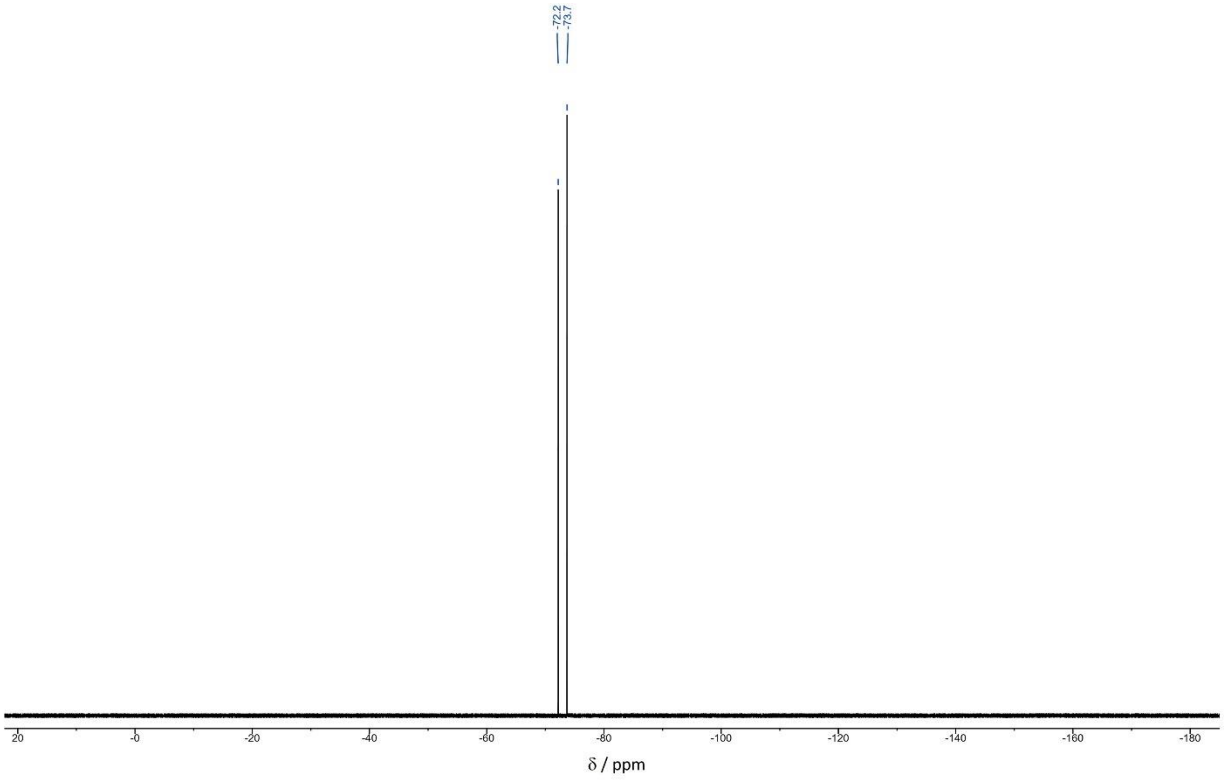

Figure S7. ^{19}F NMR spectrum (470 MHz, CD_3CN, 298K) of compound *EE*-**3**.

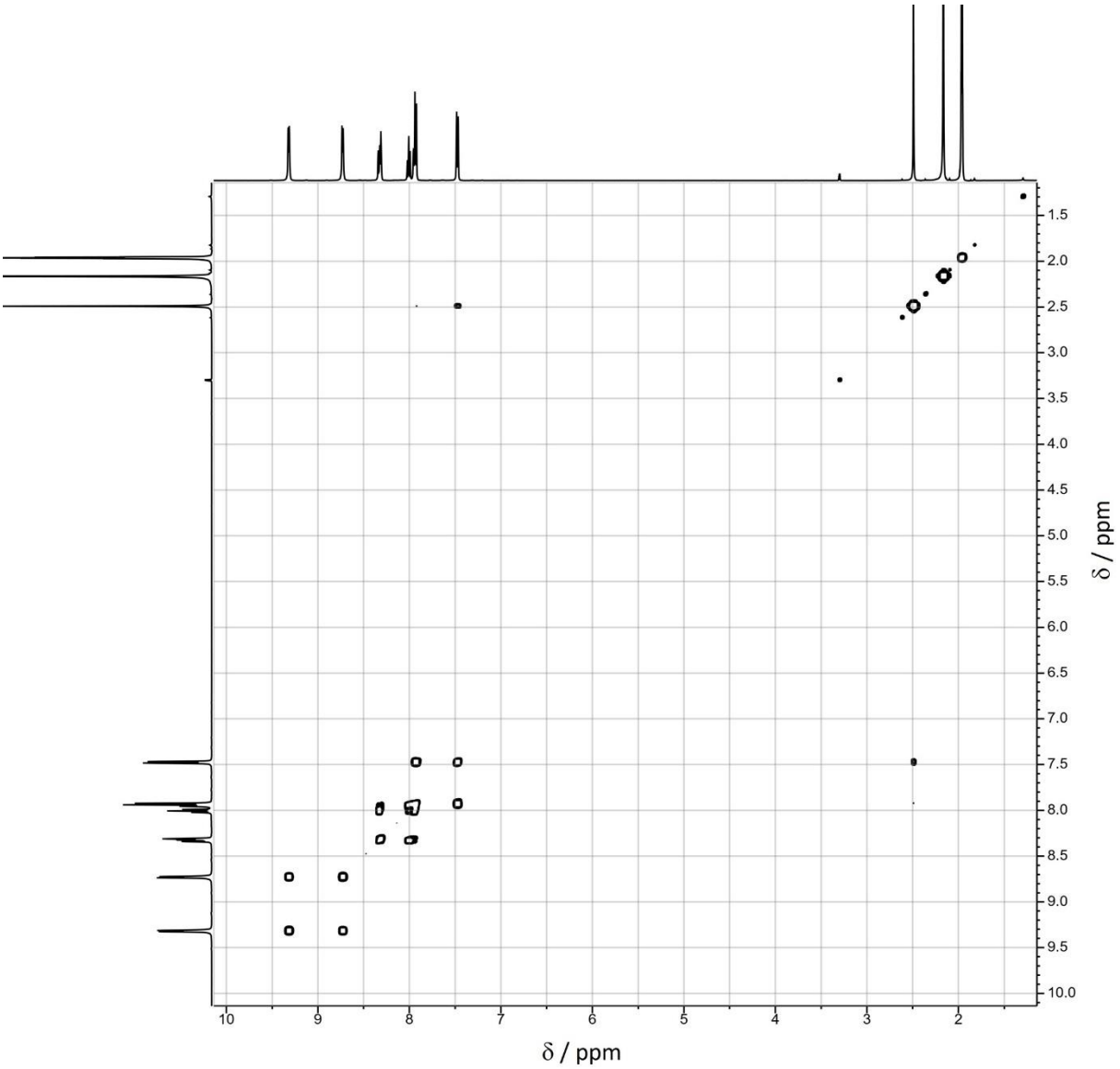

Figure S8. ^{1}H-^{1}H COSY spectrum (500 MHz, CD_3CN, 298 K) of compound *EE*-**3**.

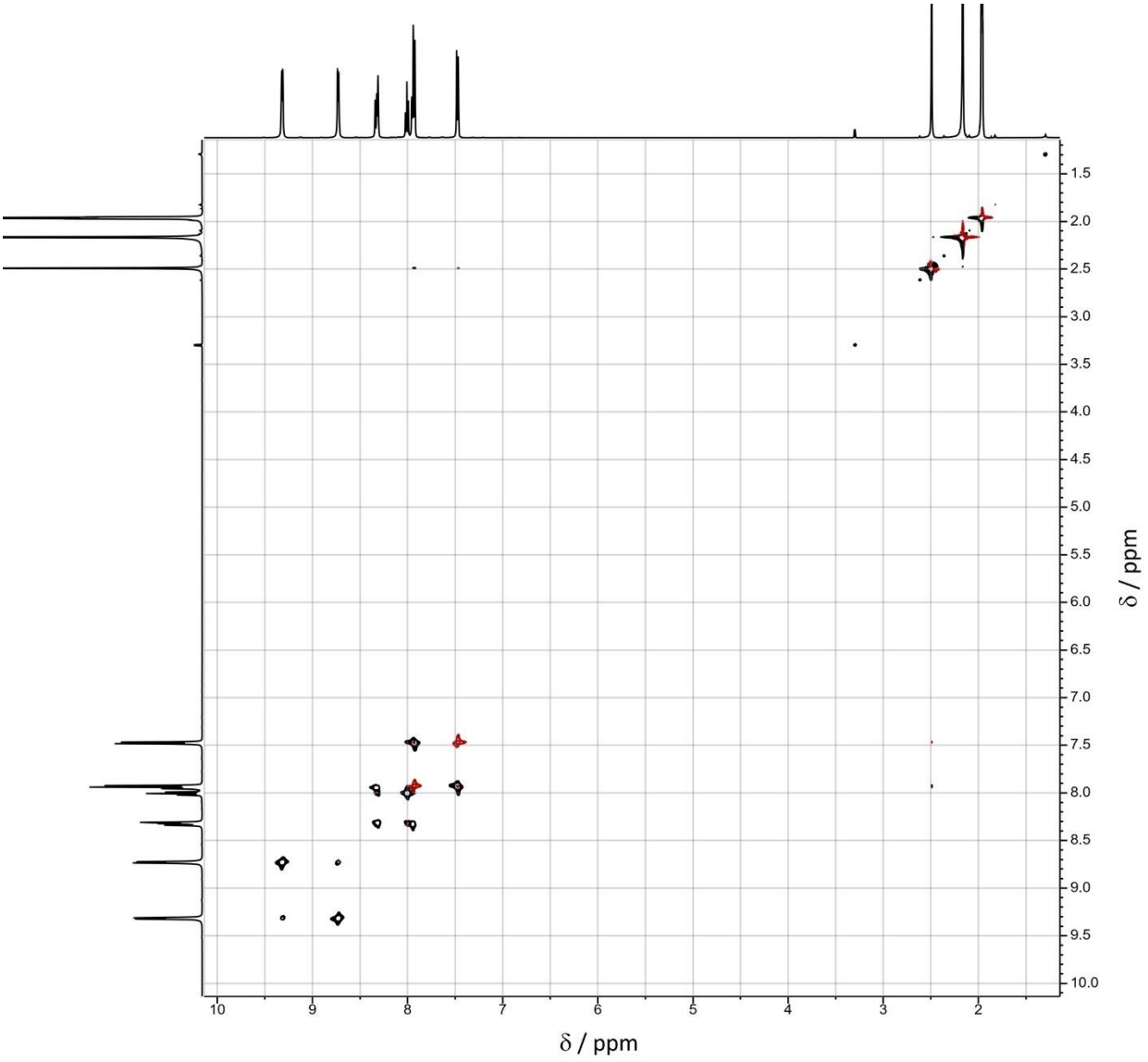

Figure S9. ^{1}H-^{1}H TOCSY spectrum (500 MHz, CD_3CN, 298 K) of compound *EE*-**3**.

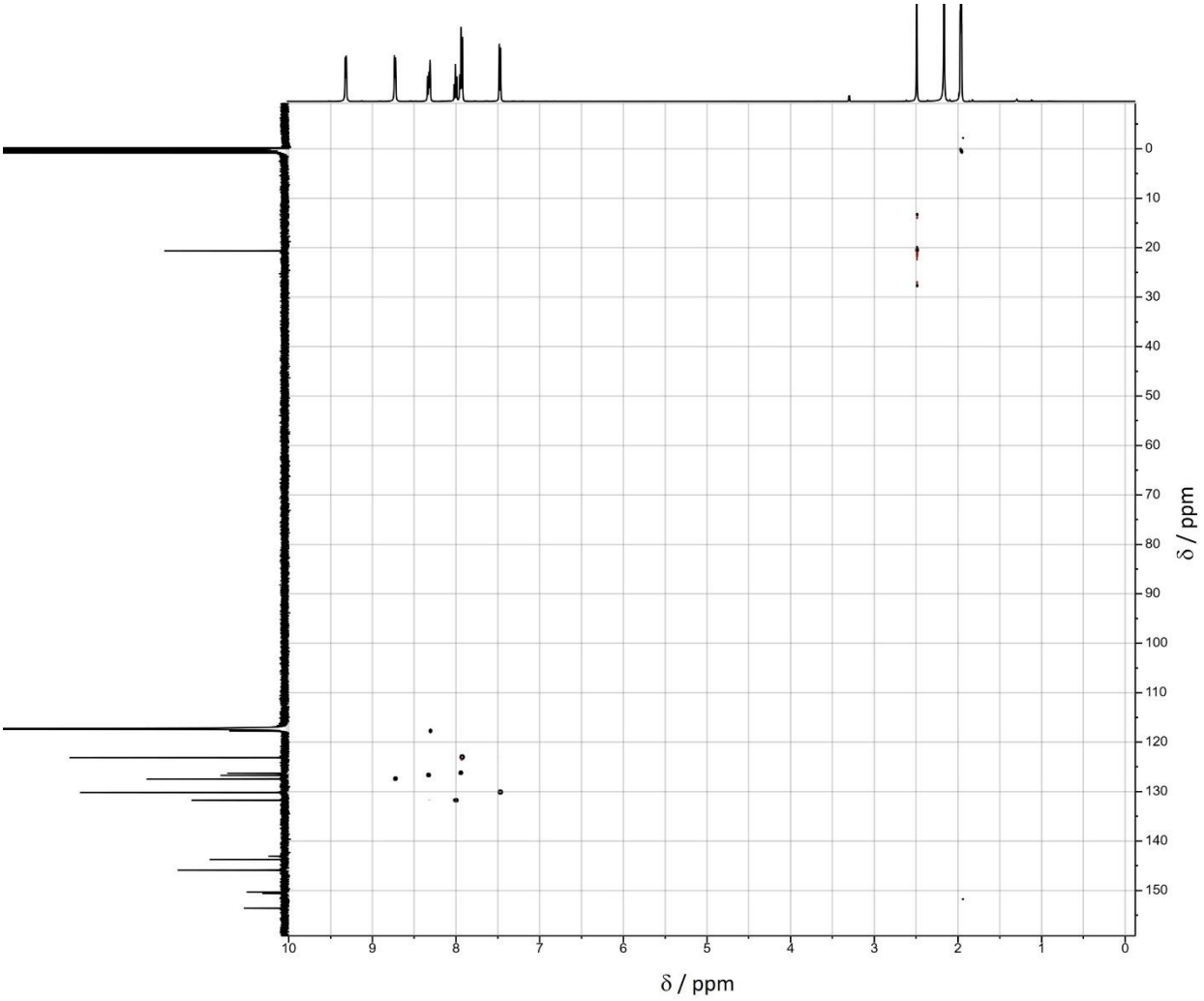

Figure S10. ^{1}H-^{13}C HSQC spectrum (500 MHz, CD_3CN, 298 K) of compound *EE*-**3**.

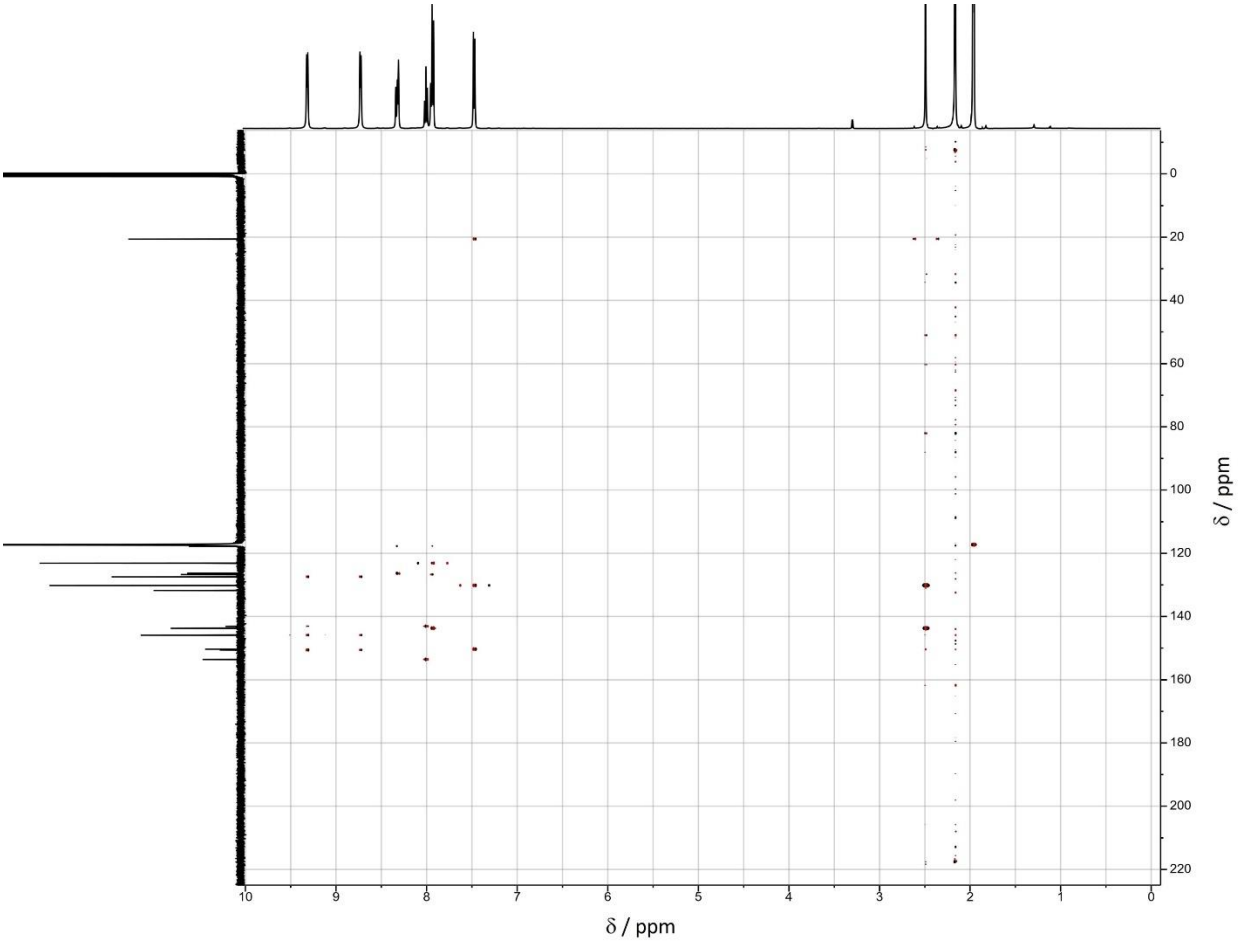

Figure S11. ^{1}H-^{13}C HMBC spectrum (500 MHz, CD_3CN, 298 K) of compound *EE*-**3**.

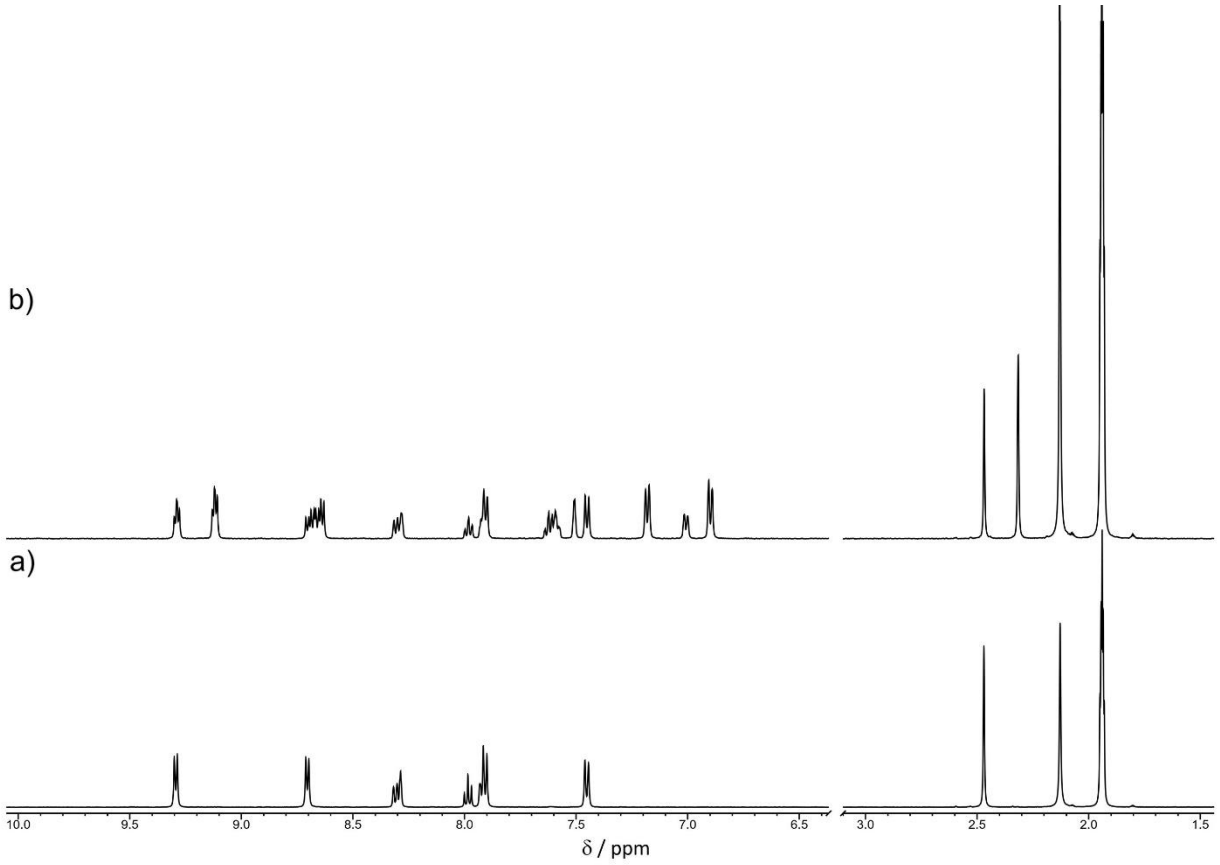

Figure S12. Partial ^{1}H NMR spectra (500 MHz, CD_3CN, 298 K) of a) compound *EE*-**3** (5mM); b) compound *EE*-**3** (5 mM) after exhaustive irradiation at λ = 369± 5 nm. Photostationary state composition (PSS): *EE* = 22 %, *EZ* = 48%, *ZZ* = 30%.

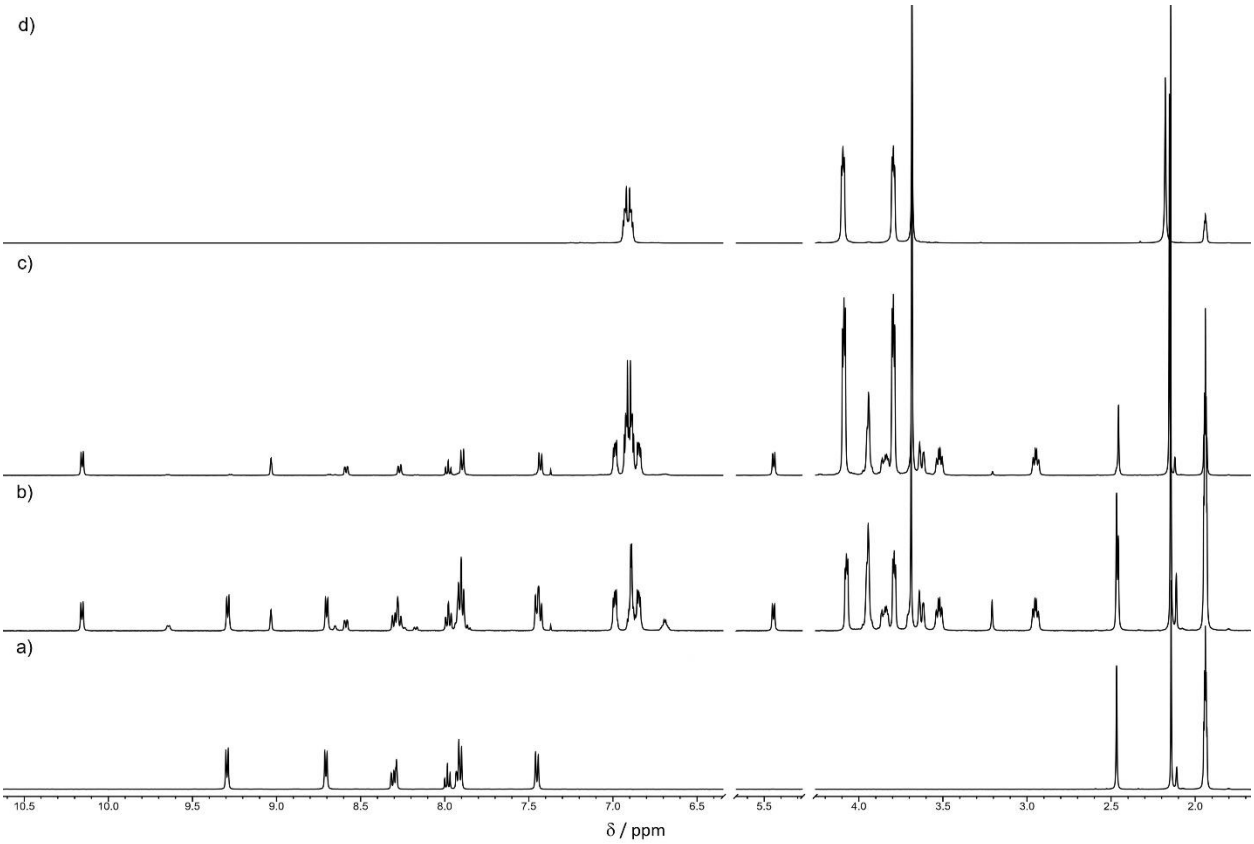

Figure S13. Partial ^{1}H NMR spectra (500 MHz, CD_3CN, 298 K) of a) compound *EE*-**3** (5 mM); *b*) solution (a) after the addition of 1.5 equivalents of **4**; c) after the addition of 6 equivalents of **4**; d) DB24C8 (10 mM).

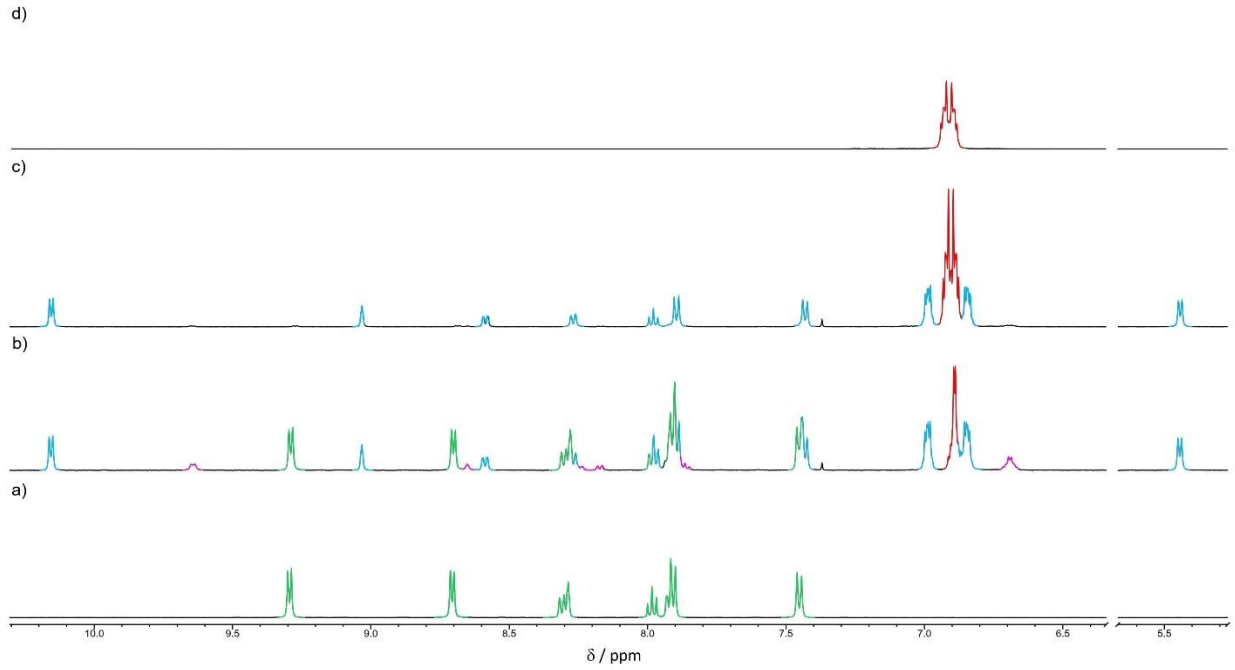

Figure S14. Partial ^{1}H NMR spectra (500 MHz, CD_3CN, 298 K) highlighting the aromatic protons signals of a) compound *EE*-**3** (5 mM); b) solution (a) after the addition of 1.5 equivalents of **4**; c) after the addition of 6 equivalents of **4**; d) **4** (10 mM). Signals are color coded to indicate: free *EE*-**3**: green, free **4**: red, *EE*-**3**⊂**4**: pink, *EE*-**3**⊂(**4**)$_2$: cyan.

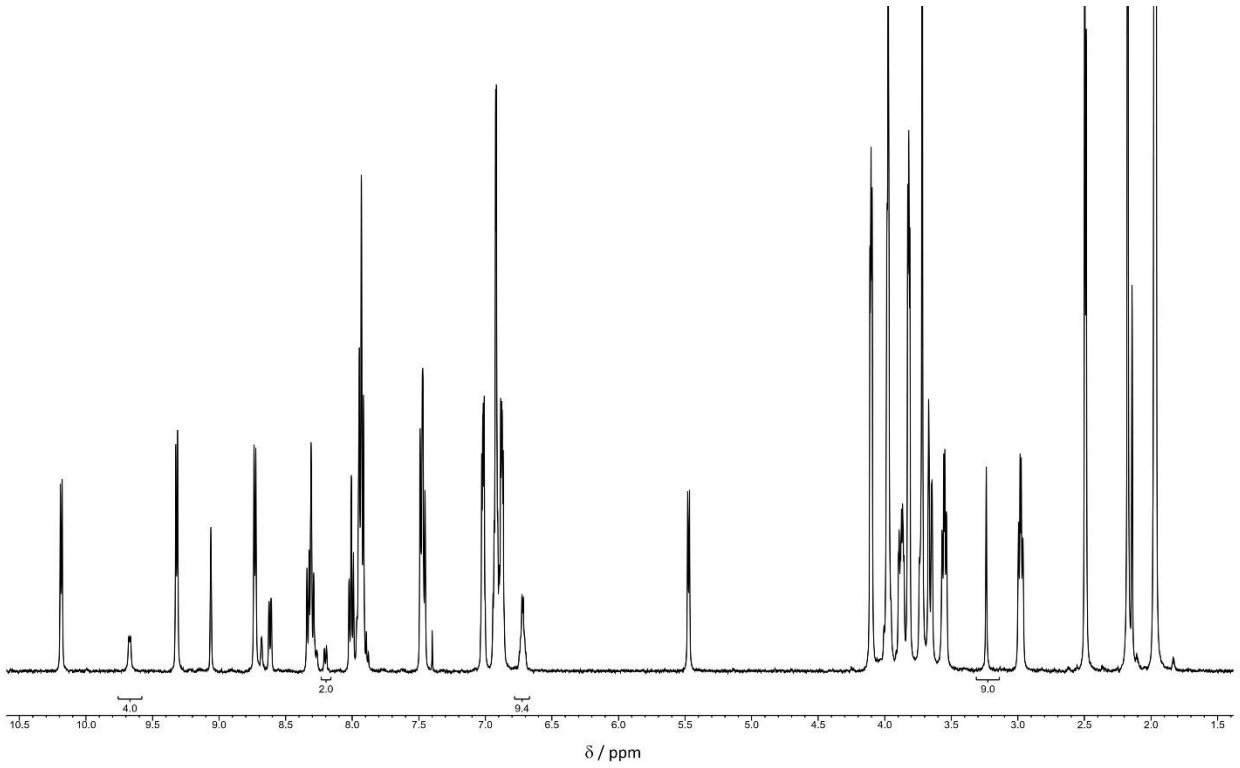

Figure S15. ^{1}H NMR spectra (500 MHz, CD_3CN, 298 K) of a 1:1.5 mixture of *EE*-**3** and **4** reporting the integrals of the peaks unambiguously assigned to complex *EE*-**3**⊂**4**, showing the 1:1 ratio between components in the [2]pseudorotaxane.

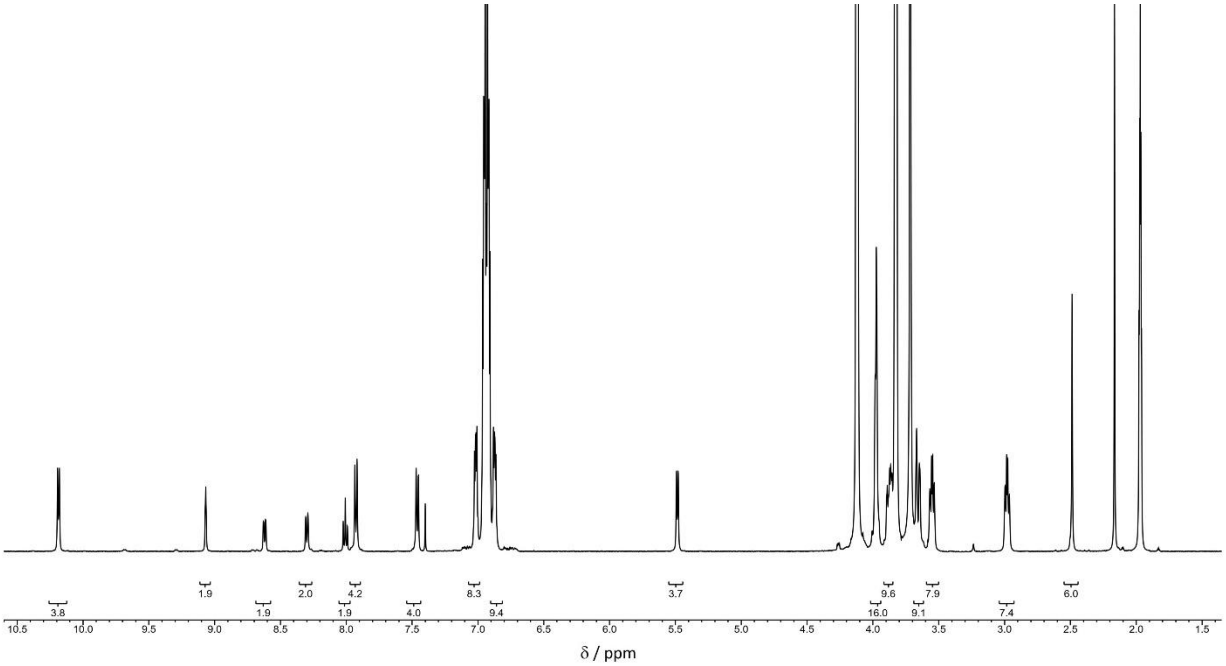

Figure S16. ^{1}H NMR spectra (500 MHz, CD_3CN, 298 K) of a 1:10 mixture of *EE*-**3** and **4** reporting the integrals of the peaks assigned to complex *EE*-**3**⊂(**4**)$_2$, showing the 1:2 ratio between components in the [3]pseudorotaxane.

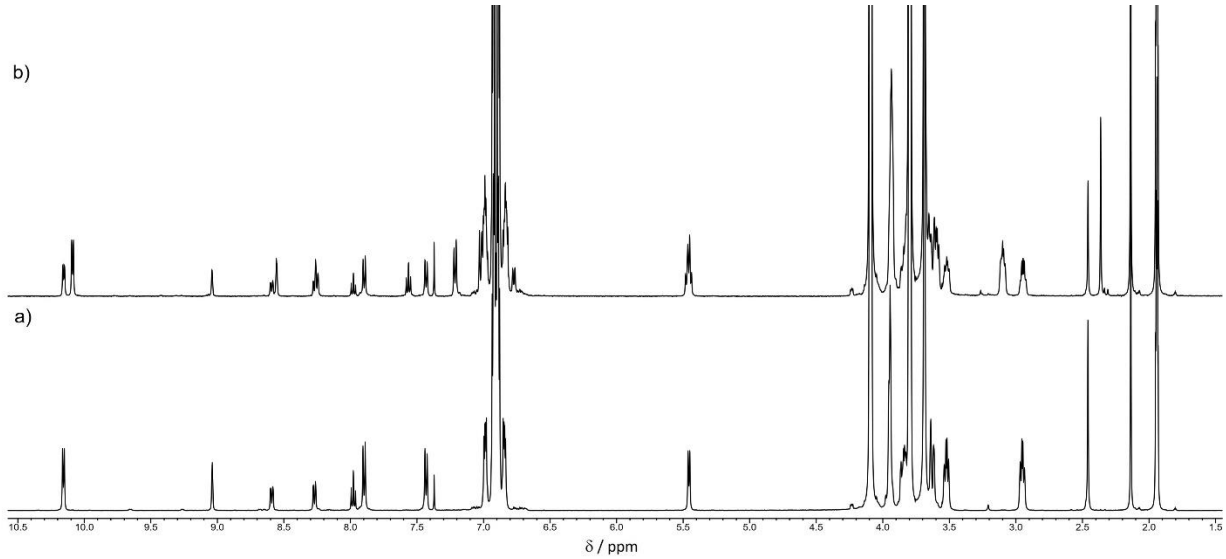

Figure S17. Partial ^{1}H NMR spectra (500 MHz, CD_3CN, 298 K) of a) a solution of *EE*-**3** (5 mM) after the addition of 10 equivalents of **4**; b) solution (a) after exhaustive irradiation at $\lambda = 369 \pm 5$ nm.

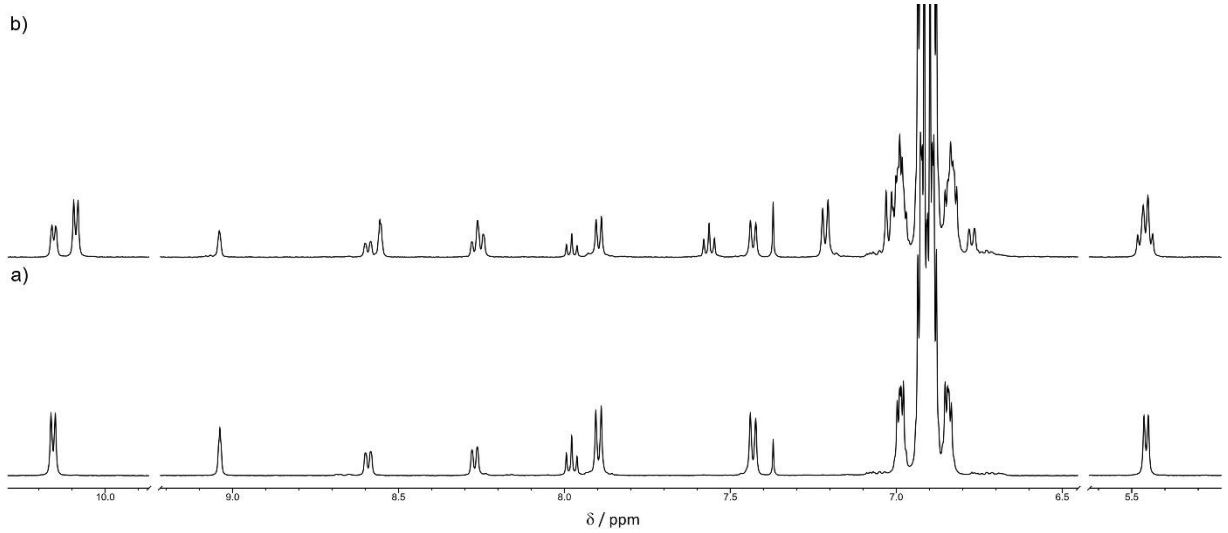

Figure S18. Partial ^{1}H NMR spectra (500 MHz, CD_3CN, 298 K) highlighting the aromatic protons signals of a) a solution of *EE*-**3** (5 mM) after the addition of 10 equivalents of **4**; b) solution (a) after exhaustive irradiation at λ = 369± 5 nm.

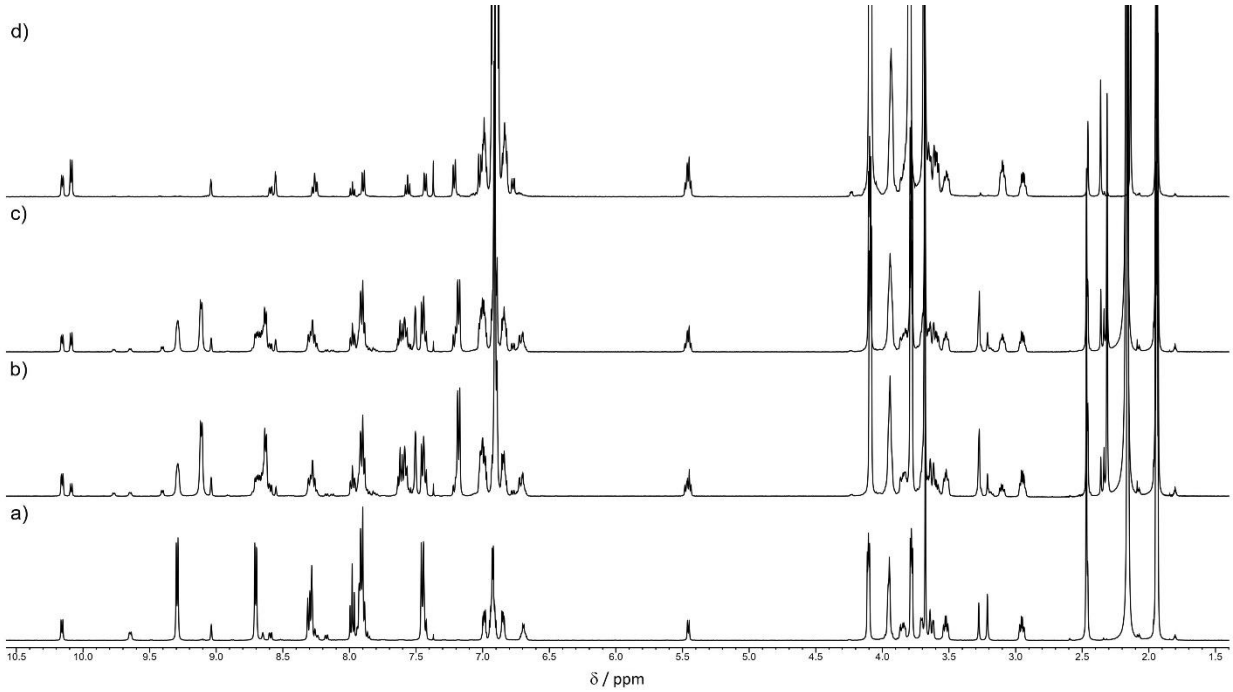

Figure S19. Partial ^{1}H NMR spectra (500 MHz, CD_3CN, 298 K) of a) a solution of *EE*-**3** (5 mM) after the addition of 1 equivalent of **4**; b) a solution of *EE*-**3** (5 mM) irradiation at λ = 369± 5 nm to reach PSS, followed by addition of 1 equivalent of **4** at t = 300 s; c) a solution of *EE*-**3** (5 mM) irradiation at λ = 369± 5 nm to reach PSS, followed by addition of 1 equivalent of **4** at t = 18000 s; d)) a solution of *EE*-**3** (5 mM) after the addition of 10 equivalents of **4** and after exhaustive irradiation at λ = 369± 5 nm.

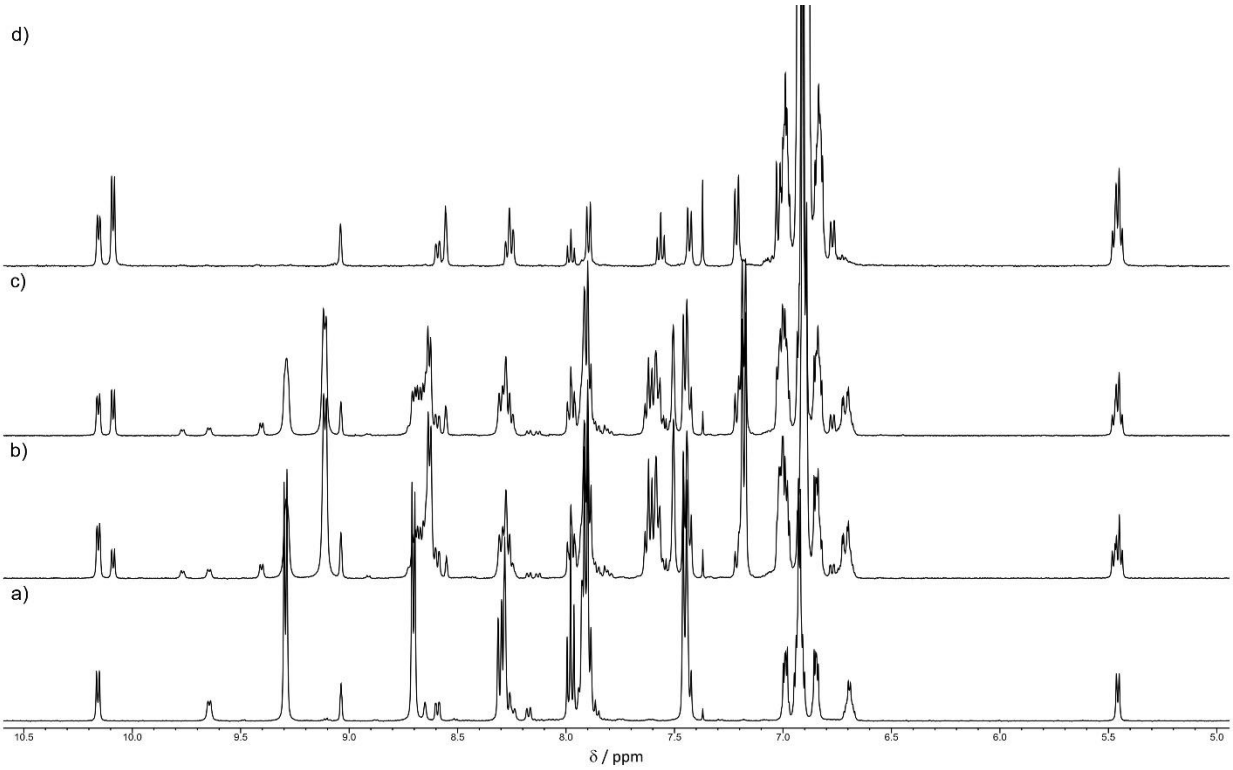

Figure S20. Partial ^{1}H NMR spectra (500 MHz, CD_3CN, 298 K) highlighting the aromatic protons signals of a) a solution of *EE*-**3** (5 mM) after the addition of 1 equivalent of **4**; b) a solution of *EE*-**3** (5 mM) irradiation at λ = 369± 5 nm to reach PSS, followed by addition of 1 equivalent of **4** at t = 300 s; c) a solution of *EE*-**3** (5 mM) irradiation at λ = 369± 5 nm to reach PSS, followed by addition of 1 equivalent of **4** at t = 18000 s; d)) a solution of *EE*-**3** (5 mM) after the addition of 10 equivalents of **4** and after exhaustive irradiation at λ = 369± 5 nm.

4. UV-Vis Characterization

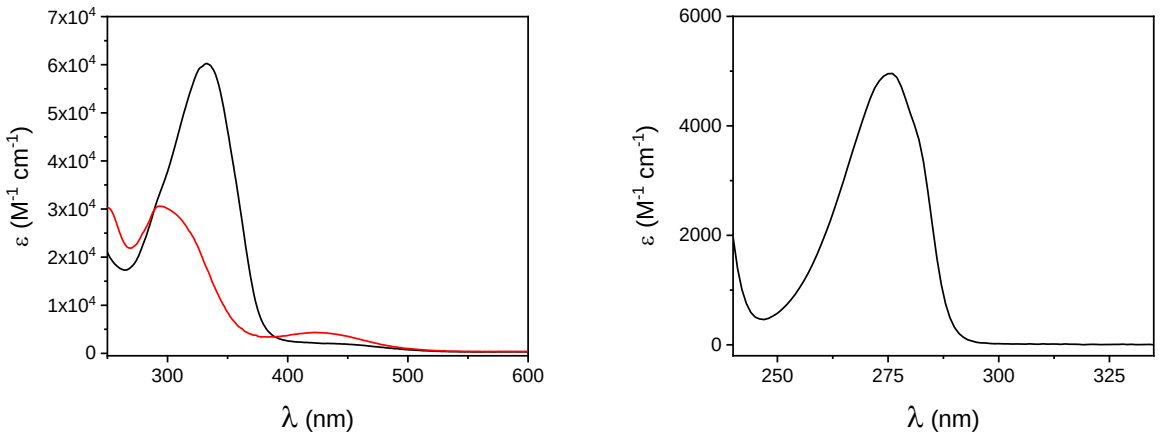

Figure S21. Left: Absorption spectrum in CH_3CN of ***EE*-3** (black line) and calculated absorption spectrum of ***ZZ*-3** (red line). Right: Absorption spectrum in CH_3CN of **4** (black line).

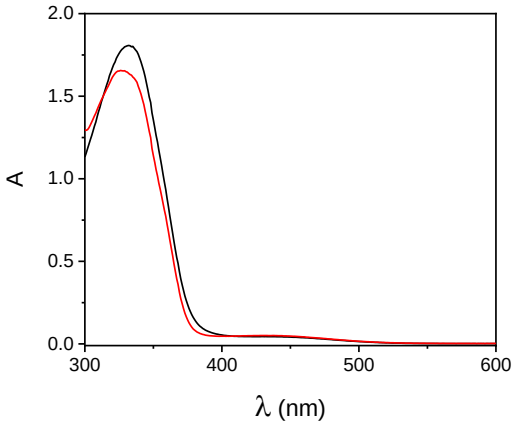

Figure S22. Absorption spectra of a CH_3CN solution of *EE*-**3** (2.8×10^{-5} M, black line) and of the same solution in presence of **4** (0.02 M, red line). In the experimental condition the majority of *EE*-**3** is associated to form the [3]pseudorotaxane (90%). Therefore, the absorption changes observed passing from the balck to the red spectrum can be correlated to the formation of the [3]pseudorotaxane.

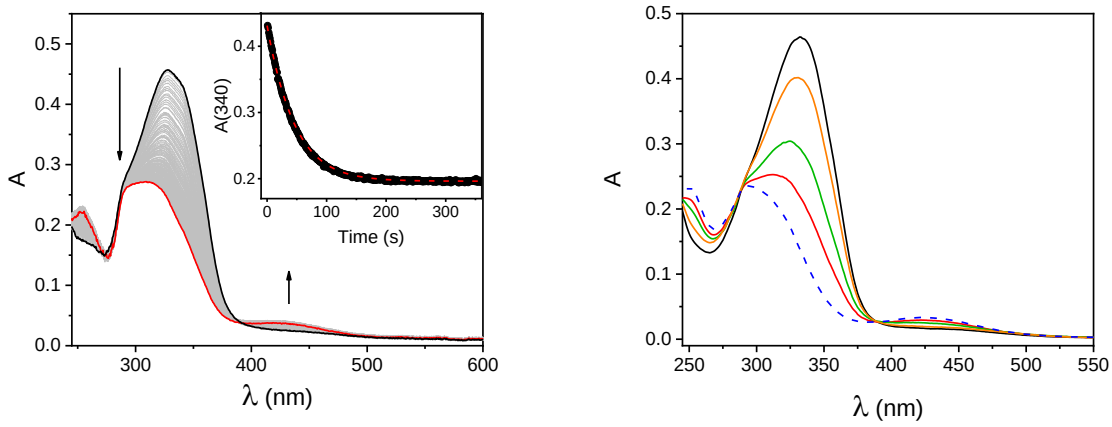

Figure S23. Left: Time-dependent absorption spectra of a CH_3CN solution of ***EE*-3** (7.6×10^{-6} M, black to red lines) upon irradiation at 365 nm. Inset: Absorption changes at 340 nm (black dots) together with the fitting of the data (red dashed line). Right: Absorption spectrum of a 7.6×10^{-6} M solution of ***EE*-3** (black line), ***ZZ*-3** (calculated, dashed blue line) and of the solution at different photostationary states: 365 nm (red line), 313 nm (green line), 436 nm (orange line).

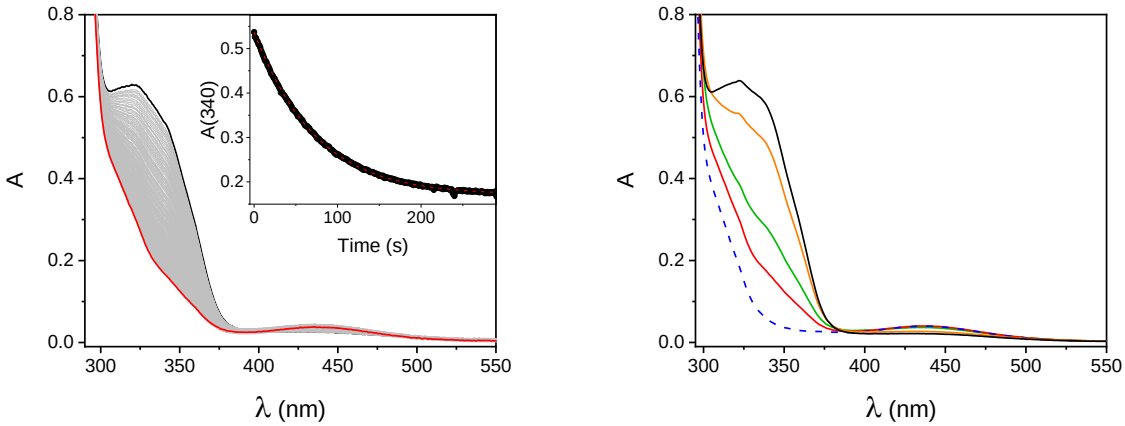

Figure S24. Time-dependent absorption spectra of a CH_3CN solution of ***EE*-3** (1.1×10^{-5} M) and **4** (0.02 M, black to red lines) upon irradiation at 365 nm. The photokinetics are fitted assuming that the amounts of free axle and [2]pseudorotaxane are negligible in the experimental conditions (<10%). Inset: Absorption changes at 340 nm (black dots) together with the fitting of the data (red dashed line). Right: Absorption spectrum of a 7.6×10^{-6} M solution of ***EE*-3** (black line), ***ZZ*-3** (calculated, dashed blue line) and of the solution at different photostationary states: 365 nm (red line), 313 nm (green line), 436 nm (orange line).

The photokinetics were fitted with a model for a T-type photochrome to determine the quantum yields for the E to Z (Φ_{EZ}) and Z to E (Φ_{ZE}) photoisomerization. This model does not take into account the presence of two identical azobenzene units in the axle and allows to fit of the experimental data. The *E* to *Z* conversion upon irradiation at 365 nm is around 75% for both ***EE*-3** and its complex with **4**, showing that both azobenzene units can be switched. Overall, these observations suggest that the photoisomeriation of one unit does not strongly affect other one, as reported for other azobenzene-based multichromophoric systems,[vi] and the two processes can be treated as independent.

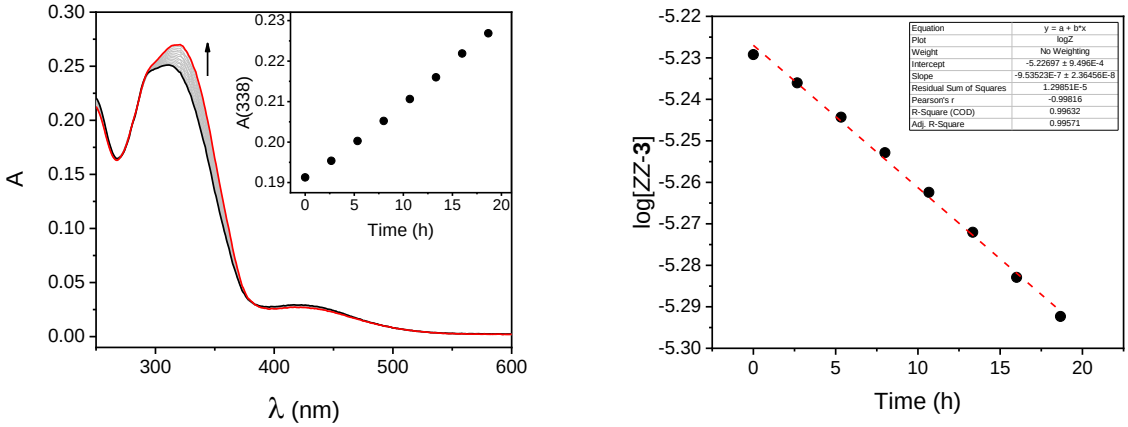

Figure S25. Left: Time-dependent absorption spectra of a CH_3CN solution of **3** (7.6×10^{-6} M, black to blue lines) previously irradiated at 365 nm. Right: Concentration changes over time of *ZZ*-**3** (black dots) together with the fitting of the data (red dashed line).

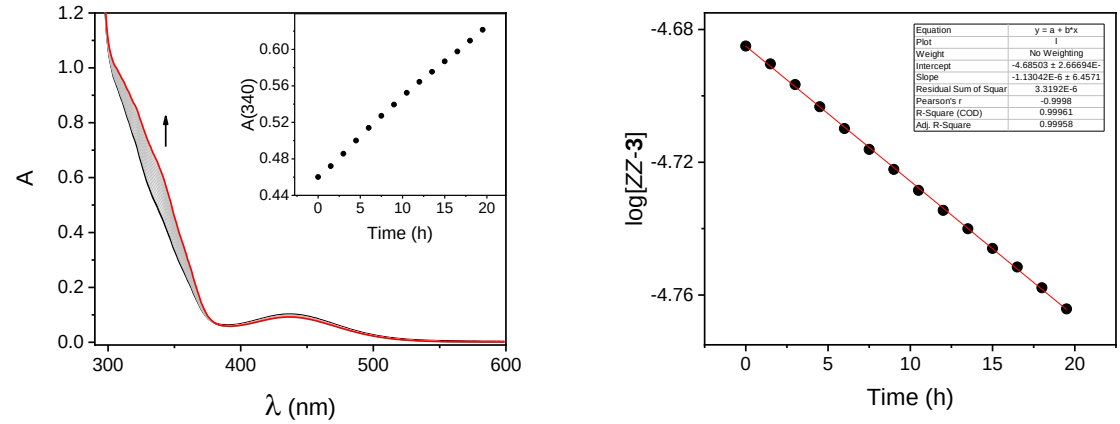

Figure S26. Left: Time-dependent absorption spectra of a CH_3CN solution of of *EE*-**3** (2.8×10^{-5} M) and **4** (0.02 M, black to red lines) previously irradiated at 365 nm. Right: Concentration changes over time of *ZZ*-**3** (black dots) together with the fitting of the data (red dashed line).

The thermal-back isomerization rate constant of *ZZ*-**3** was estimated (Fig. S16), assuming a first-order kinetics, to be $k_{th} = 1.0 \times 10^{-6}\ s^{-1}$. To do so, the logarithm of the concentration of *ZZ*-**3** over time was linearly fitted according to the equation:

$$ln[\,ZZ\text{–}\mathbf{3}] = [ZZ\text{–}\mathbf{3}]_0 - kt$$

The same experiment performed in the presence of **4** shows a similar trend (Fig. S17), with an estimated $k_{th} = 1.1 \times 10^{-6}\ s^{-1}$.

Table S1. Summary of the photochemical properties of *EE*-**3** and of the [3]pseudorotaxane *EE*-**3**⊂(**4**)$_2$ in CH_3CN at room temperature.

	Φ_{EZ} 365 nm	Φ_{ZE} 365 nm	k_{th} (s^{-1})	E : Z at PSS		
				365 nm	313 nm	436 nm
EE-**3**	6.6 %	11.9 %	1.0×10^{-6}	25 : 75	48:52	81:19
EE-**3**⊂(**4**)$_2$	6.7 %	13.8 %	1.1×10^{-6}	22 : 78	43:57	82:18

[i] A. Defoin, Synthesis, **2004**, 5, 706-710

[ii] R.-T. Wang, G.-H. Lee, C. K. Lai, J. Mater. Chem. C, **2018**, 6, 9430-9444

[iii] L. Casimiro, L. Andreoni, J. Groppi, A. Credi, R. Métivier, S. Silvi, Photochem. Photobiol. Sci., **2022**, 21, 825–833

[iv] K. Stranius, and K. Börjesson, *Sci Rep*, 2017, **7**, 41145

[v] https://berkeley-madonna.myshopify.com/

[vi] a) M. Baroncini, S. Silvi, M. Venturi, A. Credi, Chem. Eur. J. **2010**, 16, 11580 – 11587; b) M. Baroncini, S. d'Agostino, S., G. Bergamini *et al.*, *Nature Chem* **2015**, 7, 634–640